ZAAC
Zeitschrift für anorganische und allgemeine Chemie

Check for updates

Special Collection

Quantitative Scrolling into Microporous Nanotubes of the Hydrous Layered Silicate Ilerite

Felix Uhlig,[a] Ingmar Pietsch,[a] Alexander Stich,[a] Ulrich Mansfeld,[b] Sabine Rosenfeldt,[c] Jürgen Senker,*[d] and Josef Breu*[a]

Dedicated to Professor Rhett Kempe on the occasion of his 60th birthday.

The synthetic hydrous layered silicate ilerite was quantitatively converted into microporous nanoscrolls (NS). Delamination of ilerite that was ion-exchanged for N-Methyl-D-glucaminium (Meg$^+$), through one-dimensional (1D) dissolution initially yields lamellar liquid crystalline (nematic) suspensions. Subsequent protonation with acetic acid of tangling Si-O$^-$ to silanol groups reduces the pH-dependent charge of the basal surfaces. Complete NS formation is then triggered by diluting the nematic suspension below 0.05 wt%. As scrolling commonly has been attributed to hydrophobic interaction of organic counterions, Meg$^+$ was replaced by lithium ions but this showed no detrimental effect on the scrolling efficiency. The resulting NS have a typical length of 2–4 μm that corresponds well with typical diameters of the parent nanosheets. Ar-physisorption isotherms showed a bimodal micropore size with maxima around 0.8 and 1.9 nm. We attribute the first to the tubular hollow inner diameter of the NS and the latter to wedgelike interparticle porosity. The material showed a large specific surface area of 226 m^{2}g^{-1}.

[a] F. Uhlig, I. Pietsch, A. Stich, Prof. Dr. J. Breu
Faculty of Biology, Chemistry & Earth Sciences
Chair of Inorganic Colloids for Electrochemical Energy Storage
University of Bayreuth
95440 Bayreuth, Germany
E-mail: josef.breu@uni-bayreuth.de

[b] Dr. U. Mansfeld
Bavarian Polymer Institute
Physical Chemistry I
University of Bayreuth
95440 Bayreuth, Germany
E-mail: ulrich.mansfeld@uni-bayreuth.de

[c] Dr. S. Rosenfeldt
Faculty of Biology, Chemistry & Earth Sciences
Physical Chemistry I
University of Bayreuth
95440 Bayreuth, Germany
E-mail: sabine.rosenfeldt@uni-bayreuth.de

[d] Prof. Dr. J. Senker
Faculty of Biology, Chemistry & Earth Sciences
Chair of Inorganic Chemistry III
University of Bayreuth
95440 Bayreuth, Germany
E-mail: Juergen.senker@uni-bayreuth.de

Special Collection

This article is part of a Special Collection dedicated to Professor Rhett Kempe on the occasion of his 60th birthday. Please see our homepage for more articles in the collection.

Introduction

The field of nanoscrolls (NS) started attracting wide attention over 20 years ago when they were first described for oxidic 2D-materials such as titanate-,[1,2] niobate-,[3,4] tantalate-[5] and MnO$_2$[6]-NS. Several mechanisms for the rolling of the nanosheets have been proposed. Natural minerals that form NS or tubular structures have also been known for a long time, like for halloysite, imogolite, or chrysotile. Chrysotile (white asbestos) for instance comes in scrolls and scrolling was attributed to the size-mismatch between the tetrahedral and octahedral layer of the 1:1 layered silicate.[7] More recently the class of scrolled materials was further expanded to transition metal dichalkogenide-NS. For the latter, NS, however, have to be produced by high-cost and low-yield techniques like chemical vapor deposition.[8]

NS have a variety of promising characteristics (for example band structure, surface to volume ratio) for electronic,[9] optoelectronic,[10] gas sensing[11] and catalytic applications,[1,3,12] or can be used as fibrous filler materials in nanocomposites because of their high Young's modulus.[13] A controllable, quantitative colloidal route for producing NS under mild conditions with upscaling potential requires utter delamination, which in turn requires a spontaneous process like 1D dissolution of layered materials.[14] Due to the covalent nature of the layers in two dimensions thermodynamically driven dissolution of the ionic crystal – i.e. separation of the layers – can only take place along the stacking direction. Delamination then must be followed by triggering quantitative scrolling by adjusting conditions in the nanosheet suspension appropriately.

Scrolling of more rigid phyllosilicate nanosheets with a 2:1 layer structure (synthetic hectorites) has only recently been

observed. Following the adsorption of hydrophobic cationic dyes curling and partial scrolling was observed and the scrolling yield could be improved by increasing the hydrophobicity of the dye.[15]

Potential explanations for the rolling of initially symmetric nanosheets include an asymmetric adsorption of counterions at opposing basal surfaces of individual nanosheets, structural fluctuations that break the symmetry[16] and local inhomogeneities due to interlayer water.[5] For many of the materials rolling was not complete, and unpredictable. Also, drying has been proposed to induce scrolling for MoS_2 nanosheets prepared by chemical vapor deposition after subsequent wetting.[17] In a more general approach, Sasaki et. al. showed for a variety of nanosheets, that changing the ionic strength could induce scrolling and the proposed driving factor was the self-stacking of nanosheets by back-folding, creating NS.[6] The yield of nanosheets that could be transformed into NS this way was relatively low with 10%–20%.

For the synthetic hydrous layered silicate ilerite the formation of NS could be observed by ion-exchange with dioctadecyldimethylammonium followed by a solvothermal treatment for 1 day in heptane without prior delamination.[18] However, the yield was low as the authors outlined. Ion-exchange with an excess alkyl ammonium salt led to intersalination and it was hypothesized that during solvothermal treatment the excess of intercalated salt is extracted one-sided exerting a steric pressure in the still intersalinated interlayers.

Recently, a gentle and utter delamination route has been established for ilerite, producing solely monolayer nanosheets.[19] By ion-exchange of the pristine Na^+ with the highly basic and bulky protonated amino sugar megluminium (N-Methyl-D-glucaminium (Meg^+)) spontaneous 1D dissolution yielded defect-free, high aspect nanosheets. Because of the large diameter of nanosheets ($\approx 4\,\mu m$) at high concentration nematic suspension of fully delaminated nanosheets are initially obtained. Atomic force microscopy images of some nanosheets showed, however, a tendency to roll up at the edges.[19] In this work we therefore sought appropriate conditions that trigger complete scrolling of ilerite nanosheets.

Results and Discussion

Ilerite is a hydrous layered silicate with silica tetrahedrons as the primary building unit. The layers are constructed by Q^3- and Q^4-tetrahedrons in a 1:1 ratio. The secondary building units (SBU) are star-shaped $[5^4]$ cages that form long rows in one dimension (Figure 1A). They in turn are connected to two neighbouring rows to form a 2D network. The resulting layer group $p\bar{4}m2$ has a rotary inversion axis along its normal and therefore no structure-inherent strain or dipole moment exists.[20]

The in-plane connectivity of only one Si-O-Si bond connecting the rows results in a high cross-plane flexibility as compared to other silicates or transition metal dichalcogenides.[21] Consequently, dynamic distortions should be facile and may break
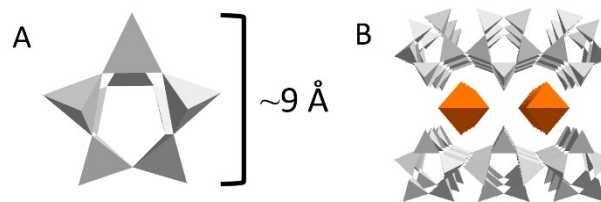

Figure 1. (A) $[5^4]$-unit built from SiO_4-tetrahedrons (grey) forming the SBU of ilerite. (B) Two mirrored sheets in the Na-ilerite structure with $Na(H_2O)_6$-octahedrons (orange) occupying the channel in the interlayer space.

the layer symmetry. This makes ilerite nanosheets the perfect model for investigating scrolling behavior.

In crystalline ilerite, two mirrored layers are stacked on top of each other, so that the tips of the $[5^4]$ cages face each other (Figure 1B). In the hollow space between the tip channels are formed. These channels are occupied by Na^+-ions, which are octahedrally coordinated by water. Looking at the structure of the complete unit cell the symmetry of the nanosheets becomes obvious (Figure S1A). The octahedrons are edge-linked forming long chains along the channels. The surface charge of ilerite sheets originates from deprotonated silanol groups of Q^3 tetrahedrons which are residing on the tip of the $[5^4]$-cages. The charge is therefore directly pH-depended and under the highly basic conditions of the synthesis (pH ≈ 12) half of the silanol groups are deprotonated. When crystalline ilerite is protonated by acid the tips and channels collapse into each other, resulting in a substantially reduced d-spacing of 7.4 Å,[22] while the thickness of a monolayer can be estimated from the crystal structure to be approximately 9 Å. This is also the d-spacing to be expected for protonated sheets that are turbostratically stacked, where the surface corrugations of neighboring layers do not match and where therefore no collapse into the channels of neighbouring sheets takes place.

As mentioned above ilerite may be fully delaminated into monolayer nanosheets by 1D dissolution. For that process to take place the interlayer sodium ions must be exchanged by the bulky organocation Meg^+. The resulting suspension of nanosheets forms a nematic suspension, where the sheets are co-facially aligned due to their high aspect ratio and the distance of the nanosheets is large and uniform because of electrostatic repulsion. It is important to note that scrolling does not occur during delamination at concentrations of above 1 wt% that was previously used to cast barrier films.[19]

This can be demonstrated by small angle X-ray scattering (SAXS), where a scaling of q^{-2} ($q < 0.1$ Å^{-1}) results from the 2D character of the nanosheets (Figure 4A(i)). The oscillations at intermediate q are attributed to interference of neighbouring ilerite sheets and correspond to d-spacings of ~18 nm.

When Meg^+ suspensions were diluted to 0.01 wt% in order to cast individualized nanosheets on substrates for characterization we frequently observed NS in scanning electron microscopy (SEM, Figure 2).
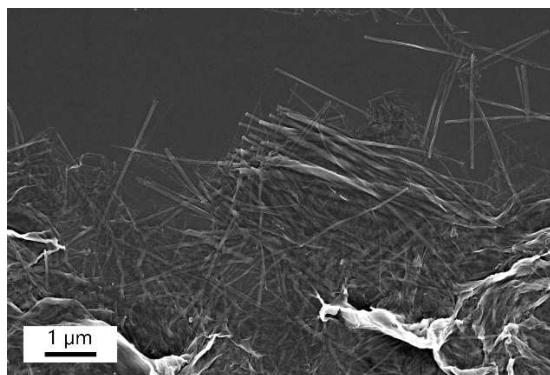
Figure 2. SEM image of a dried 0.01 wt% Meg$^+$-ilerite suspension with aggregates of NS.

As the samples for electron microscopy needed to be dried and since for MoS_2 it was reported that drying might trigger scrolling,[17] we sought to check the suspensions directly. First suspensions were cast on a lacey carbon grid and then shock-frozen by liquid ethane. Imaging these samples by cryogenic transmission electron microscopy (CryoTEM) confirms that NS are the dominating species already in dilute suspensions and that scrolling was not triggered later on during the drying process.

The NS themselves have a typical length between 2–4 μm and an outer diameter of 40 nm (Figure 3), resulting in an aspect ratio of 50–100. The length corresponds well with the diameter of the pristine square-shaped crystals (Figure S1B). At the tip of the NS, the multiple scrolled layers are stacked on top of each other suggesting the rolling happens along the sides of the square crystals rather than along the diagonal. From that can be concluded that intact nanosheets were rolled.

As several authors suggested for other NS materials that hydrophobicity of counter-cations may play a crucial role for rolling, we replaced Meg$^+$ by Li$^+$. For this the nanosheet suspension (0.1 wt%, pH = 9) was washed three times with LiCl (0.05 M) followed by concentrating the suspensions by centrifugation. The remaining organic content was below 0.5 wt%,
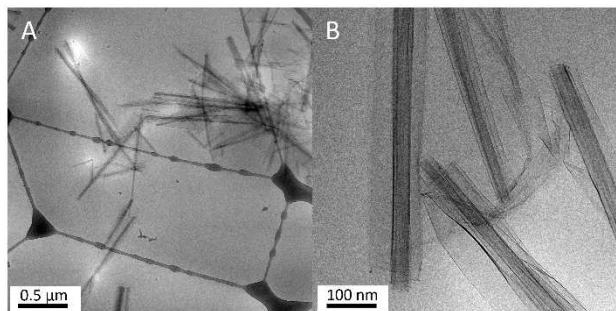
compared to 16 wt% of the pristine Meg$^+$-ilerite as determined by elemental analysis (Table S1). The ion-exchanged suspensions were then characterized by SAXS, and static light scattering (SLS). Finally, films (from a 1 wt% suspension) were cast on glass slides and the basal spacing was determined after drying by X-ray-diffraction (XRD) in Bragg-Brentano geometry. For Li$^+$-ilerite suspensions at high concentrations, the q^{-2} slope was retained, as it is expected for platelets with a nanosheet-distance of ~15 nm. Oscillations due to interference in the nematic phase are less pronounced in case of Li$^+$-ilerite, indicating smaller ordered domains (Figure 4A(ii)).

Dried films showed a d-spacing of 11.3 Å for the Li$^+$-ilerite that is substantially less than the 14.6 Å for Meg$^+$-ilerite (Figure 4B). This basal spacing is similar to crystalline Na$^+$-ilerite with a d-spacing of 11.1 Å.[20] The appearance of a *002* peak for the Li$^+$-exchanged ilerite films indicates a uniform basal spacing in the restacked monodomain films.

As already indicated by the nematic nature of the suspensions, ion-exchange did not trigger any significant aggregation as indicated also by SLS that showed a monomodal particle size distribution, which resembles that of the parent Meg$^+$-ilerite suspension (Figure S2). After successful ion exchange, the suspension was diluted (< 0.05 wt%) and drop casted on a Si wafer (Figure 4C). Nanoscrolls can be observed, therefore Meg$^+$ as bulky organo-cation appears not to be the essential driving force in NS formation. Nor does a hygroscopic Li$^+$ cation hamper scrolling in highly dilute suspensions.

As long as the charge density is kept high by maintaining a pH of 9 in the suspension, scrolling can only be trigered by dilution and never is complete as inidcated by the SAXS patterns (Figure S3) that will be discussed in some detail later.
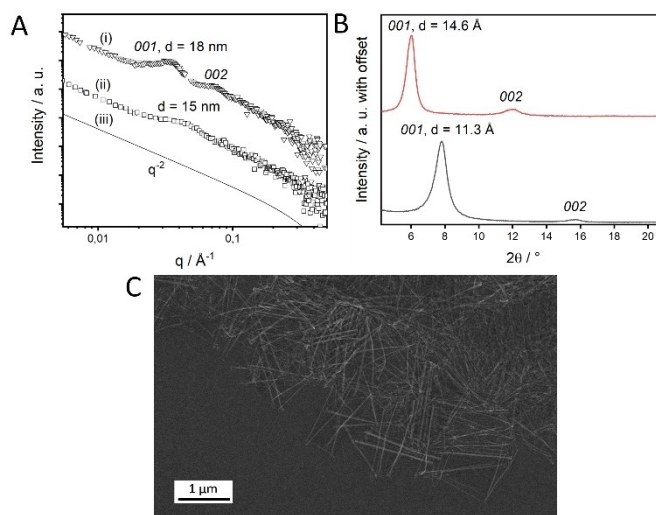

Figure 3. CryoTEM images of a highly diluted, shock-frozen Meg$^+$-ilerite suspension. (A) Wide array of NS in the frozen film. Residual dark spots and lines with beads are from the lacey carbon film support or from ice contamination. (B) Detailed image of NS.

Figure 4. (A) SAXS intensity of a Meg$^+$-ilerite ((i), 3.47 wt%), Li$^+$-ilerite ((ii), 3.84 wt%) and the theoretical intensity of an isotropic suspension of nanosheets ((iii), radius 2.0 ± 0.3 μm, thickness 9.3 ± 0.3 Å). (B) XRD of dried Meg$^+$-llerite (red) and a Li-ilerite suspension (black). (C) SEM picture of a dried < 0.05 wt% Li$^+$-ilerite suspension.

Next, the influence of the charge density on the scrolling behaviour was investigated. For this, the pH was adjusted to pH 3 by repeated washing with 0.01 M acetate solution, followed by washing with water to remove any organic remains. Given a $pK_a \approx 4.5$ for a typical Q^3 silanol group, quantitative protonation should be achieved during this process.[23] A gel was obtained by this proton exchange. Elemental analysis indicated that within experimental error Meg$^+$ was completely replaced (Tab. S1). The drop of the zetapotential from 40.7 ± 0.7 to 33.4 ± 1.1 mV corroborates a significant drop of the surface charge density of the nanosheets with protonation.

SAXS measurements after protonation indicate, that a structural change in the sample has taken place. This is shown by the absence of oscillations and by the steeper slope (Figure S3A). The change in slope hints to a more complex morphology. In contrast to the parent Meg$^+$-ilerite suspension, it could not be fitted by nematically ordered nanosheets, the slope hints to a more tubular structure as can be deduced in the comparison with the theoretical pattern for a suspension of hollow cylinders (Figure S3B).

The SAXS results are corroborated by SEM imaging for a diluted (0.5 wt%) protonated suspension, revealing fully rolled nanosheets (Figure 5A).

To probe the hollow nature of the NS, physisorption isotherms applying Ar were recorded, followed by BET analysis. A type II isotherm with a H4 hysteresis[24] was observed with a substantial micropore volume (30 cm^{3}g^{-1} with pore sizes <

15 nm). The pore size distribution is rather broad with a maximum at 0.8 nm (Figure S4), which we attribute to the inner hollow diameter of the tube. Additionally, mesoporosity was observed, which we attribute to wedgelike pores generated between individual NS in NS-aggregates. The specific surface area calculated is 226 m^{2}g^{-1} (Figure 5B), a value similar to surface areas that have been reported for titanate-NS.[25]

A dried powder of the NS suspension showed a quite sharp basal spacing 9.3 Å, which corresponds well to the d-spacing for turbostratic protonated ilerite (Figure S5).[26]

As mentioned before, Meg$^+$-ilerite belongs to a still small group of layered compounds that show spontaneous 1 D dissolution. Upon adding water to the crystalline powder lamellar liquid crystalline hydrogels are obtained. Moreover, the large diameter of the nanosheets and the high charge density holds the individual nanosheets in a coplanar orientation resulting in nematic phases even at high dilutions. With a typical diameter of 4 μm, the separation of nanosheets in the nematic phase would have to be increased to more than 1 μm corresponding to some 10^{-4} wt% before the nanosheets gain the flexibility to bend sufficiently to initiate scrolling.[27] At higher concentrations scrolling is simply hampered by steric restrictions. Moreover, the considerable negative zeta potential (40.7 ± 0.7 mV for Meg$^+$-ilerite, pH 9) impedes scrolling in addition to steric restrictions as the distance to the adjacent nanosheet is reduced by scrolling against electrostatic repulsion. Given these aspects, it is obvious that scrolling requires considerable dilution of the suspensions to the limit where the nanosheet separation is large enough to ease the steric and electrostatic restrictions. Given the same separation/dilution, a lower charge density will foster scrolling. This is seen when comparing SAXS data for Meg$^+$-ilerite and a protonated suspension that have been diluted to the same extent before reconcentration, needed for the SAXS experiments. As expected only the protonated system shows a significant deviation from the q^{-2} slope (Figure S3C), indicating that protonated NS are clearly more susceptible to scrolling. Meg$^+$-ilerite suspensions show some scrolling but the process is not complete as indicated by the q^{-2} slope. SEM and TEM micrographs are misleading as scrolls are easy to be spotted but 1 nm thin nanosheets escape unnoticed.

Scrolling of the ilerite layers in the protonated suspension induces major changes for the ^{29}Si MAS NMR spectra (Figure 5C and Figure S7). Compared to the flat layers for Meg$^+$-ilerite, a pronounced shift of the Q^3 signal by about 1.5 ppm was observed, while the chemical shifts for the Q^4 units essentially do not change. Simultaneously, the Q^3/Q^4 intensity ratio within the CP spectra, acquired for the dried suspensions (Figure 5C), changes markedly. For protonated ilerite, the Q^3 signals are favoured and roughly 2.3 times larger. This corresponds to protonation rate of the Q^3 units that is higher by roughly 70% compared to Meg$^+$-ilerite, in turn reducing the layer charge by the same amount. Additionally, the line widths for the ^{29}Si NMR spectra collected for the suspensions (Figure S7A) differ significantly. Meg$^+$-ilerite features sharp resonances for both the Q^3 and Q^4 units demonstrating a fast solvent exchange at the ilerite surfaces probably combined with a residual mobility of
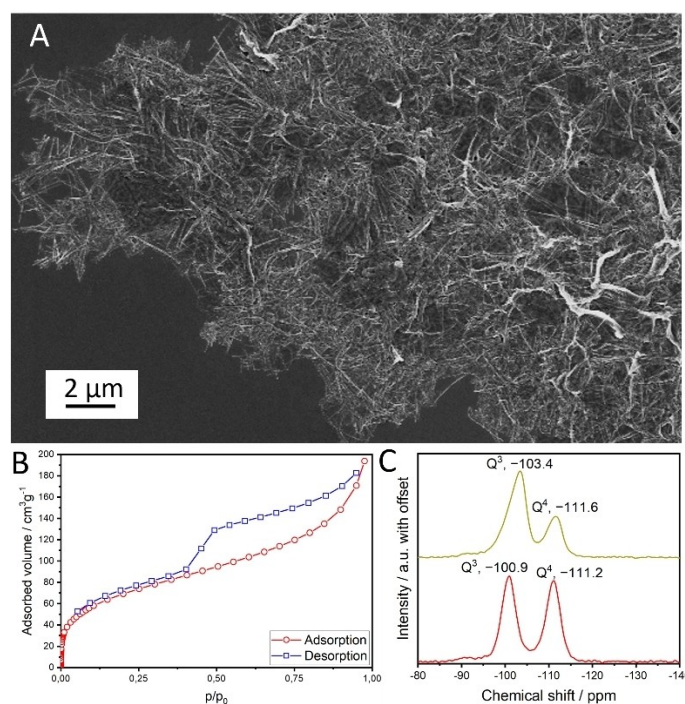

Figure 5. (A) SEM picture of a dried 0.5 wt% protonated suspension. (B) Adsorption isotherm of a dried sample of protonated suspension showing micro- and mesoporosity. (C) ^{29}Si CP NMR MAS spectra of dried protonated (green) and Meg$^+$-ilerite (red) suspensions (0.5 wt%).

the ilerite layers. In contrast, the NS in the protonated suspension lead to resonances that are 4 times broader suggesting a higher rigidity of the ilerite surfaces in the scrolled state.

Even in the dilute state scrolling will require to somehow break the symmetry and differentiate between inner and outer basal surface of the scrolled multilayer wall. For nanosheets with a centrosymmetric structure the symmetry break might be accomplished by an unbalanced distribution of counterions. The degree of unbalance required might be varying for the different types of nanosheets for which scrolling has been observed. In particular, the cross-plane stiffness is expected to have a large impact. The more force needed for bending a particular nanosheet, the stronger has the symmetry to be broken. In this respect, ilerite nanosheets as compared to for instance 2:1 layered silicates like hectorite, are expected to be rather soft and easy bendable. If by bending of the layers, the acidity of the silanolgroups is affected, protons might quickly follow the differentiated acidity of inner and outer basal surfaces.

Alternative reasons might be transient fluctuations of flexible nanosheets with organocations that offer a significant potential for van der Waals energy or hydrogen bonding when approaching each other during initial bending of the nanosheet edges. These forces between cations located on an inner and an outer surface of the same nanosheet might trigger a kind of restacking into a 1D crystal. The multiwalled NS then show basal spacings that correspond with ordinary intercalation compounds where these organocations are intercalated between coplanar monolayers. In this line for Meg^+-ilerite NS a d-spacing of 12.3 Å was observed (Figure S6) as compared to 14.6 Å for the intercalation compound. The distinct self-interaction strength might explain why scrolling for Meg^+-ilerite is incomplete while for protonated ilerite it is complete.

Conclusion

Spontaneous scrolling appears to be a common phenomenon, if not the general rule for flexible (monolayer) nanosheets once separated to large distances where steric and electrostatic restrictions for scrolling are lifted. As a general trend, scrolling seems to be fostered by low charge densities and counter ions that attract each other through van der Waals interactions and/or hydrogen bonding once inner and outer surfaces of a bent nanosheet approach each other through back bending.

For ilerite with a quite flexible layer structure NS can be obtained quantitatively simply by protonation followed by dilution to < 0.01 wt%. This renders ilerite NS a promising low-cost tubular and microporous nanomaterial that might be applied as catalyst support or as 1D filler in composite materials. The silanolgroups accessible at the outer and inner diameter, moreover, allow further functionalization via silylation chemistry.

Experimental Section

Experimental SectionSynthesis of ilerite

Ilerite has been synthesized according to the literature.[23] NaOH-pellets ($\geq$ 98%, Sigma-Aldrich), colloidal SiO_2 (30 wt%, Köstrosol 1030 KD), and double-distilled water were mixed under vigorous stirring resulting in a $Na_2O:SiO_2:H_2O$ molar ratio of 1:4:37. The synthesis was carried out in a teflon-lined steel autoclave at 100 °C for 21 d. The product was washed with distilled water and dried at 40 °C.

Meglumin-exchange

The meglumin exchange was performed by subsequent washing procedures with 1 M meglumine solution, adjusted to pH 9 with concentrated HCl. The resulting slurry was washed with double-distilled water until a transparent gel of 2 wt% was obtained.[19]

Protonation of a nematic suspension

For protonation 1 ml of gel was washed 3 times with 0.01 M acetic acid (99.9%, VWR Chemicals) for 1 h, followed by washing in double-distilled water 2 times for 1 h to remove residual meglumi-nium and excess acetic acid. After drying at 80 °C typically 10 mg powder are obtained (~90% yield in silica content).

Li^+-exchange of a nematic suspension

For the Li^+-exchange of the suspension, 1 ml of the gel was washed with 0.05 M LiCl-solution 3 times for 1 h followed by washing in double-distilled water 2 times for 1 h.

X-ray diffraction

Textured samples were measured in Bragg-Brentano geometry on a PANalytical Empyrean diffractometer with a Cu $K_{\alpha1}$ radiation equipped with a PixCel1D-Medipix3 detector.

Small-angle X-ray scattering

SAXS data were measured using a "Double Ganesha AIR" (SAXSLAB/Xenocs). The X-ray source of this laboratory-based system is a rotating copper anode (MicroMax 007HF, Rigaku Corporation, Japan). The data were recorded by a position-sensitive detector (PILATUS 300 K, Dectris). The suspensions were measured in 1-mm glass capillaries. The circularly averaged data are normalized to the incident beam, sample thickness, and measurement time. Background subtraction was performed by using the SAXS pattern of a water-filled capillary for the suspensions.

For further evaluation the software Scatter (Version 2.5)[28] or SasView (Version 4.2.2).[29]

Cryogenic transmission electron microscopy

CryoTEM measurements were performed on a JEOL JEM 2200FS operating at 200 kV. Images were recorded with a CMOS OneView camera (Gatan, US). For cryo preparation, freshly prepared samples were diluted to 0.01 wt% and vortexed for 30 s. A Cu grid with a lacey carbon film (200 mesh, Plano GmbH, Germany) was glow-discharged prior the deposition of 4 μL of the solution at 5 °C and 100% humidity. Subsequently, the grid was blotted with filter paper and plunge-frozen in liquid ethane using a Leica EM GP

plunge freezer (Leica, Germany). After preparation, the grid was stored in liquid nitrogen, transferred, and imaged at temperatures below −170 °C.

Scanning electron microscopy

Scanning electron microscope images were recorded on a Zeiss 1530.

Elemental analysis

An Elementar Unicube equipped with a combustion tube filled with tungsten (VI) oxide granules was used at a combustion temperature of 1050 °C.

Argon physisorption measurements

Argon physisorption isotherms were recorded using a Quantachrome Autosorb 1 at Ar(l) temperature (87.35 K). The Autosorb 1 was equipped with the CryoSync cryostat (Quantachrome). The samples were dried for 24 h at 80 °C in high vacuum before measuring. The data were analyzed using the ASiQwin software package (Version 3.0). Pore sizes and volumes were derived using NLDFT based on spherical/cylindrical pore models for zeolite/silica materials.

Zeta-potential measurements

Zeta-potential was measured with a Malvern Zetasizer Nano ZS.

^{29}Si NMR MAS

All samples were measured with a spectrometer Bruker Avance III 400 (Magnetic Field 9.4 T) in a 3.2 mm MAS triple resonance probe (Bruker) at a spinning speed of 10.0 kHz. To obtain the ^{29}Si CP NMR MAS spectra a ramped cross-polarization experiment was used, where the nutation frequency on the proton channel was varied linearly by 50 %. The corresponding nutation frequency on the ^{29}Si channel and the contact time were adjusted to 50 kHz and 8 ms, respectively. The ^{29}Si NMR MAS spectra were acquired using a quantitative onepulse – experiment with a 90° pulse length of 3.8 μs. The recycle delays were set to 600 s for the powder samples and 5 s/60 s for the gels. For both techniques proton broadband decoupling was applied during acquisition using a spinal-64 sequence with a nutation frequency = 70 kHz. The ^{29}Si spectra are referenced indirectly with respect to tetramethylsilane (TMS).

Acknowledgements

Conflict of Interest

The authors declare no conflict of interest.

Data Availability Statement

The data that support the findings of this study are available from the corresponding author upon reasonable request.

[1] D. V. Bavykin, F. C. Walsh, *Eur. J. Inorg. Chem.* **2009**, *2009*, 977–997.

[2] D. A. Sheppard, C. E. Buckley, Australia, **2005**.

[3] R. Ma, Y. Kobayashi, W. J. Youngblood, T. E. Mallouk, *J. Mater. Chem.* **2008**, *18*, 5982.

[4] G. B. Saupe, C. C. Waraksa, H.-N. Kim, Y. J. Han, D. M. Kaschak, D. M. Skinner, T. E. Mallouk, *Chem. Mater.* **2000**, *12*, 1556–1562.

[5] R. E. Schaak, T. E. Mallouk, *Chem. Mater.* **2000**, *12*, 3427–3434.

[6] R. Ma, Y. Bando, T. Sasaki, *J. Phys. Chem. B* **2004**, *108*, 2115–2119.

[7] J. Niu, in *Developments in Clay Science, Vol. 7* (Eds.: P. Yuan, A. Thill, F. Bergaya), Elsevier, **2016**, pp. 387–408.

[8] S. Aftab, M. Z. Iqbal, Y. S. Rim, *Small* **2023**, *19*, 2205418.

[9] X. Xie, M.-Q. Zhao, B. Anasori, K. Maleski, C. E. Ren, J. Li, B. W. Byles, E. Pomerantseva, G. Wang, Y. Gogotsi, *Nano Energy* **2016**, *26*, 513–523.

[10] I. Milošević, B. Nikolić, E. Dobardžić, M. Damnjanović, I. Popov, G. Seifert, *Phys. Rev. B* **2007**, *76*, 233414.

[11] T. Allsop, R. Arif, R. Neal, K. Kalli, V. Kundrát, A. Rozhin, P. Culverhouse, D. J. Webb, *Light-Sci. Appl.* **2016**, *5*, e16036-e16036.

[12] K. Woan, G. Pyrgiotakis, W. Sigmund, *Adv. Mater.* **2009**, *21*, 2233–2239.

[13] a) A. Krasilin, M. Khalisov, E. Khrapova, V. Ugolkov, A. Enyashin, A. Ankudinov, *Materials* **2022**, *15*, 9023; b) A. A. Krasilin, M. M. Khalisov, E. K. Khrapova, T. S. Kunkel, D. A. Kozlov, N. M. Anuchin, A. N. Enyashin, A. V. Ankudinov, *Part. Part. Syst. Charact.* **2021**, *38*, 2100153.

[14] V. Dudko, O. Khoruzhenko, S. Weiß, M. Daab, P. Loch, W. Schwieger, J. Breu, *Adv. Mater. Technol.* **2023**, *8*, 2200553.

[15] Y. S. Takumi Harada, T. Nakato, J. Kawamata, *Scientific Research Abstracts* **2023**, *14*, 111. https://euroclay.aipea.org/download/book-of-abstracts/ (accessed 2023-06-28).

[16] R. E. Schaak, T. E. Mallouk, *J. Am. Chem. Soc.* **2000**, *122*, 2798–2803.

[17] Y. Zhao, H. You, X. Li, C. Pei, X. Huang, H. Li, *ACS Appl. Mater. Interfaces* **2022**, *14*, 9515–9524.

[18] Y. Asakura, M. Sugihara, T. Hirohashi, A. Torimoto, T. Matsumoto, M. Koike, Y. Kuroda, H. Wada, A. Shimojima, K. Kuroda, *Nanoscale* **2019**, *11*, 12924–12931.

[19] P. Loch, D. Schuchardt, G. Algara-Siller, P. Markus, K. Ottermann, S. Rosenfeldt, T. Lunkenbein, W. Schwieger, G. Papastavrou, J. Breu, *Science Advances*, *8*, 20.

[20] S. Vortmann, J. Rius, S. Siegmann, H. Gies, *J. Phys. Chem. B* **1997**, *101*, 1292–1297.

[21] H. Sato, A. Yamagishi, K. Kawamura, *J. Phys. Chem. B* **2001**, *105*, 7990–7997.

[22] M. Borowski, B. Marler, H. Gies, *Z. Kristallogr.* **2002**, *217*, 233–241.

[23] G. Borbély, H. K. Beyer, H. G. Karge, W. Schwieger, A. Brandt, K. H. Bergk, *Clays Clay Miner.* **1991**, *39*, 490–497.

[24] M. Thommes, K. Kaneko, A. V. Neimark, J. P. Olivier, F. Rodriguez-Reinoso, J. Rouquerol, K. S. W. Sing, *Pure Appl. Chem.* **2015**, *87*, 1051–1069.

[25] A. Kleinhammes, G. W. Wagner, H. Kulkarni, Y. Jia, Q. Zhang, L.-C. Qin, Y. Wu, *Chem. Phys. Lett.* **2005**, *411*, 81–85.

[26] M. Borowski, B. Marler, H. Gies, *Z. Kristallogr. – Cryst. Mater.* **2002**, *217*, 233–241.

[27] S. Rosenfeldt, M. Stöter, M. Schlenk, T. Martin, R. Q. Albuquerque, S. Förster, J. Breu, *Langmuir* **2016**, *32*, 10582–10588.

[28] S. Förster, S. Fischer, K. Zielske, C. Schellbach, M. Sztucki, P. Lindner, J. Perlich, *Adv. Colloid Interface Sci.* **2011**, *163*, 53–83.

[29] M. Doucet, J. H. Cho, G. Alina, J. Bakker, W. Bouwman, P. Butler, K. Campbell, M. Gonzales, R. Heenan, A. Jackson, P. Juhas, S. King, P. Kienzle, J. Krzywon, A. Markvardsen, T. Nielsen, L. O'Driscoll, W. Potrzebowski, R. Ferraz Leal, T. Richter, P. Rozycko, T. Snow, A. Washington, Zenodo, **2019**.